Journal of Nano Research
ISSN: 1661-9897, Vol. 80, pp 81-96

Submitted: 2023-05-08
Revised: 2023-07-12
Accepted: 2023-07-14
Online: 2023-09-05

Stabilized Bare Superparamagnetic Iron Oxide Nanoparticles: Synthesis and Characterization

E.K. Suter[1,a]*, H.L. Rutto[1,a], W.N. Omwoyo[2,b], Musamba Banza[1,a]

[1]Department of Chemical Engineering, Vaal University of Technology, South Africa.

[2]Chemistry Department, Vaal University of Technology, South Africa. Private Bag X021, Vanderbijlpark, 1900 Andries Potgeiter Blvd.

[a]esuter78@gmail.com, [b]hilaryr@vut.ac.za, [c]wesleyomwoyo16@gmail.com, [d]banzajeanclaude@gmail.com
*Corresponding author: Evans Suter,
E-mail address: esuter78@gmail.com

Keywords: stabilized, magnetic, iron oxide, nanoparticles, co-precipitation

Abstract. Iron is a ubiquitous element found on Earth's crust, existing in various forms, such as Magnetite (Fe_3O_4) and Hematite (α-Fe_2O_3). Magnetic iron oxide nanoparticles (MIONPs) have become increasingly popular because they possess unique properties such as high surface area to volume ratio, super-paramagnetic properties, photocatalytic properties, and economical synthesis methods. This study produced MIONPs using the co-precipitation method, stabilized by a molybdenum magnet. Two soluble iron salts ($FeCl_3.6H_2O$ and $FeSO_4.7H_2O$) were reacted with 5N NH_4OH solution at 80 °C in a nitrogen atmosphere. The MIONPs had a high saturation magnetization of 74.2emu/g, good crystallinity with crystalline spinel structured magnetite phase of iron oxide, high thermal stability depicted by 2.09 wt. % weight loss, and small particle sizes (6-25 nm). FTIR revealed a high-intensity peak at 546.28 cm^{-1}, attributed to the Fe-O stretching bond. Furthermore, the study showed that the co-precipitation method could be used to produce nanoparticles with a wide range of properties that could be used for various applications. It is a promising solution for producing stabilized magnetic nanoparticles since it uses non-toxic reagents and a straightforward, secure technique. Therefore, it may be used to synthesize nanoparticles for targeted treatment, magnetic resonance imaging, drug delivery, water treatment purposes and environmental remediation.

1.0 Introduction

Nanotechnology has seen rapid advances in recent years, leading to immense technological improvements, in manufacturing, telecommunication, health, environmental remediation, electronics, etc. [1–3]. It involves producing and utilizing nanomaterials, which are substances with sizes ranging from 1-100 nm [4, 5]. These materials possess unique properties not found in their larger versions [6, 7]. Examples of nanomaterials include carbon-based nanomaterials, such as single-walled carbon nanotubes (SWCNTs) with a cylindrical shape and a single sheet of graphene, and multi-walled carbon nanotubes (MWCNTs) consisting of multiple layers of graphene sheets [8], as well as TiO_2 nanomaterials, which exist naturally in three crystalline forms (anatase, rutile, and brookite) and can be produced using biological agents [9, 10]. Most of these nanomaterials including iron nanoparticles have been extensively studied and reviewed.

Iron is one of the most common elements on Earth's crust. In its oxidized form, it exists in various forms, two of the most prominent being Magnetite (Fe_3O_4) and Hematite (α-Fe_2O_3) [11,12]. Magnetic iron oxide nanoparticles (MIONPs) have become increasingly popular due to their unique properties, such as their high surface area-to-volume ratio, super-paramagnetic properties, photocatalytic properties, economic and environmental friendly synthesis methods [13]. The MIONPs further offer unprecedented versatility in applications due to their ability to be modified, coated with various materials like polymers, lipids, silica, and gold, among others, and manipulated on an atomic scale [14]. Furthermore, they are biocompatible, chemically inert, and environmentally friendly, making

them ideal for combining with various biotechnological products like proteins, antibodies, peptides, nucleic acids, etc. [15].

Researchers have been exploring physical and chemical methods to synthesize iron nanoparticles with specific properties [16]. Different structures have been produced, such as nano-belts, nano-rings, nano-ovals, and other nanostructures [17,18]. Advances in instrumentation have made it possible to synthesize nanomaterials with precise sizes, controlled active sites, and mono-dispersed and well-controlled iron oxide nanoparticles [19].

Synthesis of MIONPs can be achieved through various methods such as sonochemical, mechanochemical, co-precipitation, and biologically mediated methods. The sonochemical process involves the dispersion of the metal ions or cells in an aqueous media through hydrodynamic mechanical treatment. It entails the generation of efficient cavitation's; implosion, expansion, and formation of microscopic gas bubbles due to the application of ultrasonic energy [20]. The action of the hydrodynamic forces of the ultrasound on the metal ions leads to the dispersion and disintegration of metal nanoparticles [21].

In the co-precipitation technique, reactions between salts with various solubilities in water are regulated by factors including pH and temperature. This technique uses two or more water-soluble salts that interact with one another [22]. As a result of the reaction, one or more water-insoluble salts are created in the liquid phase, and precipitation occurs when the product concentration exceeds the solubility product value in the reaction media [23]. The co-precipitation process has numerous advantages, such as a high yield, high product purity, the lack of a requirement for organic solvents, ease of replication, and low cost of production. In this process, newly generated ions form a shell around the core by precipitating on its surfaces instead of dissolving in the solution [24, 25].

Mechanochemical synthesis occurs at the boundaries of continually regenerating, nanometre-sized grains and allows chemical reactions to proceed at low temperatures in a ball mill without external heating [26]. By choosing appropriate milling settings and adding inert diluents, nanocrystalline particles can be created within a soluble salt matrix. Subsequent washing with the right solvents selectively removes the matrix phase, resulting in agglomeration-free nanoparticles [27]. However, this method consumes a significant amount of energy during the combustion process to enhance the milling process [28]. Biological-mediated techniques utilizing bacteria and fungi have also been employed for nanoparticle synthesis. Iron-reducing bacteria, such as *Actinobacter sp*., have been used to produce spherical iron oxide nanoparticles in an aerobic setting [29]. The bacteria produce iron reductase enzymes that facilitate the synthesis process, resulting in nanoparticles with diameters ranging from 40 to 60 nm [30, 31]. Fungi-mediated synthesis involves using different fungi species such as; *P. chlamydosporium, A. fumigates, A. wentii, C. lunata, and C. globosum,* etc. with a mixture of ferric and ferrous salts at room temperature. The fungi secrete proteins that enhance the hydrolysis of iron complexes, leading to the formation of crystalline magnetite particles [32, 33]. Various fungi species have been tested for the production of iron nanoparticles, but this method can be complex, costly, and require proper handling [34, 35].

This present study utilized co-precipitation method. The co-precipitation method influenced by a molybdenum magnet as a precipitating stabilizer was chosen for this study due to its relative simplicity and cost-effectiveness. The process does not require high temperatures or pressures and allows for forming iron oxide crystals with uniform size and shape. Since the process is simple, it can be scaled up to larger batches, making it suitable for industrial applications. Furthermore, the method was selected since it does not produce any hazardous by-products, making it a safe and environmentally friendly method for synthesizing iron oxide nanoparticles.

2.0 Materials and Methods

2.1 Chemicals

Iron (III) chloride hexahydrate ($FeCl_3.6H_2O$) (≥99%), ammonium hydroxide (5N, NH_4OH), ferrous sulfate heptahydrate ($FeSO_4.7H_2O$) (≥99.5%), Molybdenum magnet, and methanol (≥99.85%). All

chemicals were purchased from Sigma-Aldrich, Merck-South Africa. The chemicals were used as received. The entire experiment was carried out using deionized water.

2.2 Methods

2.2.1 Synthesis of MIONPs by Co-precipitation

The synthesis of MIONPs followed the schematic procedure shown in Fig.1. To synthesize MIONPs, 100 mL of deionized water was transferred to a three-neck round-bottomed flask fitted with a Liebig condenser and a magnetic stirrer. To establish an inert atmosphere, the deionized water was degassed by heating it to 80 °C and bubbling nitrogen gas through for 15 minutes. To the oxygen-free water, 3.1 g of ferric chloride hexahydrate and 2.1 g of ferrous sulfate heptahydrate salts were introduced and stirred vigorously for 1 hour with the temperature maintained at 80 °C. Thereafter, 5N of NH_4OH solution was added dropwise for co-precipitation, and the mixture was stirred for an additional 1 hour until the color turned dark brown, where the pH of the solution was 11.3. The residue was allowed to settle with the help of a molybdenum magnet as a stabilizer for 30 min at room temperature to prevent sedimentation of the unreacted impurities on the formed MIONPs. It was then rinsed multiple times with a deionized water-methanol solution and separated using a centrifuge set at 5000 rpm, the supernatant was then discarded. The resulting pure precipitate was dried overnight at 60 °C in a vacuum desiccator. It was then kept in airtight sample holders for characterization.

Fig.1. Flow diagram for the synthesis of MIONPs

2.3 Characterization

2.3.1. Ultraviolet-Visible (UV-Vis) spectroscopy

The UV-Vis spectrum was scanned between 200 nm to 600 nm wavelengths using JASSCO-V 650 UV-Visible Spectrometer. Before the analysis, the nanoparticles were dissolved in toluene and placed in a 1 cm path-length quartz cuvette. The spectrophotometer was set to a wavelength range of 200 to 600 nm, and toluene was used as the reference solvent. The measurements were then taken, and the results were recorded.

2.3.2. Photoluminescence (PL) Spectroscopy

Photoluminescence (PL) was carried out to understand the illumination of the absorption and emission spectrum of the prepared MIONPs. A xenon lamp and a Perkin Elmer 45 Photoluminescence (PL) spectrometer were used to capture the MIONPs emission spectra at room temperature. The sample was placed in a 1 cm glass cuvette with toluene as the solvent.

2.3.3 Vibrating sample magnetometer

The vibrating sample magnetometer- 7404 (VSM) was used to measure the magnetic characteristics of the synthesized magnetite nanoparticles in response to an applied magnetic field.

2.3.4 Fourier Transform Infrared Spectroscopy (FTIR)

FTIR spectroscopy and a Nicolet iS50 FT-IR spectrophotometer (Thermo Nicolet, USA) was used to identify the functional groups of the MIONPs to explore their structural alterations. The FTIR transmittance mode spectrum of MIONPs was recorded from 4000 cm^{-1} to 500 cm^{-1}. The resulting spectrum was pre-treated with baseline subtraction using a polynomial fitting approach to determine the MIONPs functional group information.

2.3.5 Thermal properties

Perkin Elmer Pyris 1 Thermogravimetric Analyzer (TGA) was used to measure the mass loss of MIONPs under a carefully regulated temperature shift. 11.00 mg of MIONPs sample was placed into the TGA sample holder, then heated in a nitrogen environment from 30 °C to 1000 °C at a rate of 10 °C/min. The % weight loss was recorded as the temperature rose.

2.3.6 Transmission Electron Microscopy (TEM)

The size and structure of the prepared MIONPs were evaluated using a Tecnai G2 20 S-Twin Transmission Electron Microscope. A thin copper grid with a carbon covering was employed with a 0.1%wt. MIONPs suspension. After drying, the sample was tested at an accelerating voltage of between 100 and 120 kV. This method allowed for a complete investigation of the MIONPs, giving details about their characteristics and possible interactions with their surroundings.

2.3.7 Surface morphology

The morphology of the MIONPs has been examined using scanning electron microscopy (SEM). The photos were captured using a JEOL- JSM 7500F Field Emission Scanning Electron Microscope. To prepare the sample for imaging, a gold sputtering procedure was used to cover the MIONPs, and carbon film was used as the sample holder. The SEM imaging allowed us direct examination of the MIONPs' morphological characteristics.

2.3.8 X-Ray Diffraction Analysis

Shimadzu-XRD 700 X-ray diffractometer generated XRD patterns with Cu Ka radiation (λ =0.1539 nm). The scan rate was set to 1 Hz, the current was set to 30 mA, and the voltage was set to 40 kV. After loading the samples into the sample holder, they were put into the XRD slot, and measurements were collected and recorded. As shown in equation 1 below, the crystal size (D) was determined using Scherer's equation, which takes into consideration the dimensionless form factor (K), the X-ray wavelength (λ), the line broadening at half maximum intensity (FWHM) (β), and the Braggs angle (θ) [36].

$$Crystal\ Size\ (D) = \frac{K\lambda}{\beta\ Cos\ \theta} \qquad (1)$$

2.3.9 Elemental Analysis

An Electron Diffraction Spectrum (EDS) EOL JEM 2100 LaB6, (JEOL Ltd., Tokyo, Japan) analysis was carried out to quantify the composition of various elements present in the prepared MIONPs.

3.0 Results and Discussions

3.1 Physicochemical characteristics MIONPs

The physical appearances of the precursor reagents and the synthesized MIONPs are captured in Fig. 2. As shown in Fig. 2, the pure salts of iron (III) chloride hexahydrate yellow in color (2a), and Ferrous sulfate heptahydrate is blue (2b). The co-precipitated MIONPs are dark brown (2c). Iron (III) chloride

(2a) is yellow because it contains iron ions in a trivalent state which absorbs the visible spectrum of light in the visible region [37]. Due to the existence of an anionic species termed ferrocyanide ($Fe_4[Fe(CN)_6]^{3-}$), which is a by-product of the interaction between ferric ions (Fe^{3+}) and ferrocyanide ions ($Fe_4[Fe(CN)_6]^{3-}$), the ferrous sulfate heptahydrate appears blue. Prussian blue reaction is a typical occurrence in ferrous sulfate heptahydrate solutions [38].

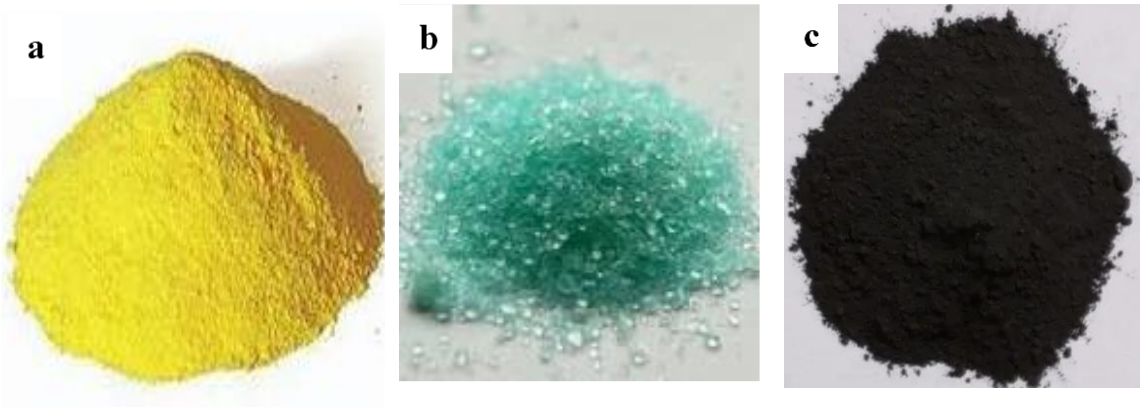

Fig. 2. Physical appearances of (a) iron (III) chloride hexahydrate (b) Ferrous sulfate heptahydrate and (c) MIONPs

The treatment of the iron solution with ammonium hydroxide led to the formation of a dark brown precipitate (Fe_3O_4) which is the MIONPs Fig. 2c. The addition of precipitating agent such as NaOH to the solution was to reduce the iron ions present in the zero-valent state making it to attain the magnetization [39].

3.2 UV-Visible Spectroscopy

Optical absorption spectra depend upon factors like oxygen vacancies, impurities in the MNIOPs, band gap, and crystal morphology. The produced MIONPs were dispersed in ethanol and then cleaned with deionized water before being analyzed using UV-Vis spectroscopy. Fig. 3, shows the UV-Vis spectrum with a peak at 276 nm wavelength, which is a typical absorption band of iron oxide nanoparticles [40]. The characterization results demonstrated that the particles had the expected peak at 276 nm, indicating that the sample comprised iron oxide nanoparticles.

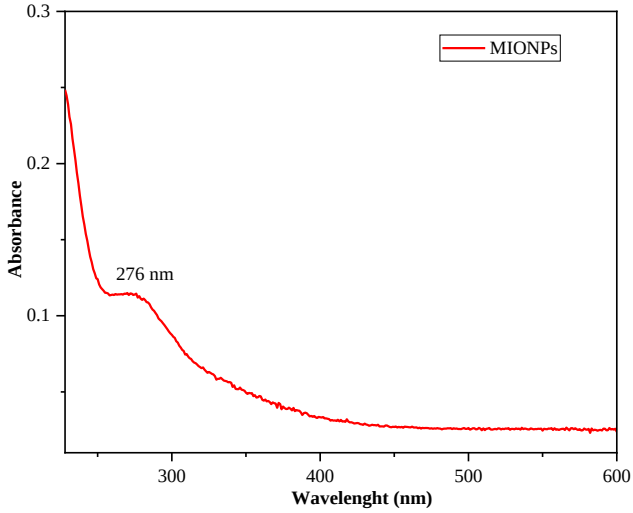

Fig. 3. UV-Vis spectroscopy of MIONPs

3.3 Photoluminescence

The photoluminescence (PL) spectrum of the prepared iron oxide nanoparticles (MIONPs) synthesized via co-precipitation, with an excitation wavelength of 540 nm, is shown in Fig. 4. The emission peak is observed at 411 nm, indicating far UV band edge emissions and UV band intensity

due to better crystallinity. It is hypothesized that the local d-band transition property of Fe_3O_4 boosts the magnetic coupling of nearby Fe^{3+} ions, which leads to the photoluminescence and the alteration in oxygen atomic coordinates and the rise in the Fe-O bonding gap [41]. The technique of synthesis used for MIONPs is critical in keeping the photoluminescent characteristics. The synthesis process utilized effectively restricted the broadening of the electron wave function by blocking energy interaction between the environment and the nanoparticles. This restriction of the wave function, in turn, helped to the stabilization of the bound excitations, resulting in the observed photoluminescence, showing that the MIONPs produced were more stable against external variables such as energy exchange. The significant Stokes shift between the emission peak and the excitation wavelength suggests that the emission is likely due to a bound-exciton source. This is further supported by the synthesis method, which prevents the environment and nanoparticles from exchanging energy, thus inhibiting the widening of the electron wave function [32, 42].

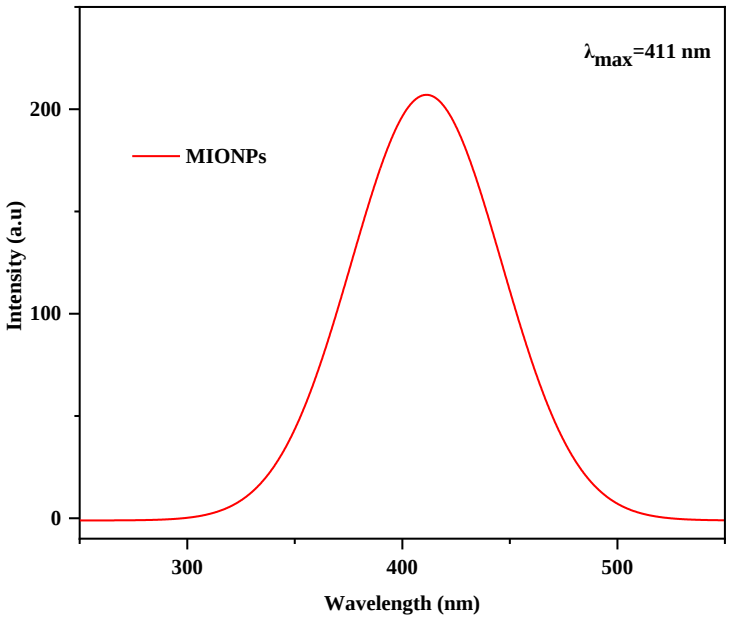

Fig. 4: Photoluminescence Emission Spectrum of MIONPs

3.4 Magnetic properties

The magnetic characteristics of the produced nanoparticles in response to an applied magnetic field are shown in Fig. 5. The lack of hysteresis, remanence, and coercivity in the synthesized magnetite nanoparticles was a sign of regular superparamagnetic activity and nature of the MIONPs produced during the molybdenum assisted co-precipitation [43]. Large saturation magnetization is a well-known indicator of maximal magnetic strength [44]. Compared to the theoretical value of 92 emu/g, the saturation magnetization of the produced magnetite particles was determined to be equivalent to 74.2 emu/g [45]. This research established that the MIONPs could respond quickly to external magnetic fields and had outstanding magnetic characteristics. It is interesting to note that the excellent magnetic properties of the nanoparticles were discovered to be influenced by the stabilizing effect of a molybdenum magnet used during the precipitation process [46]. The higher magnetic field potential of the nanoparticles was probably caused by the molybdenum magnet's influence on the size, shape, and magnetic behaviour of the particles.

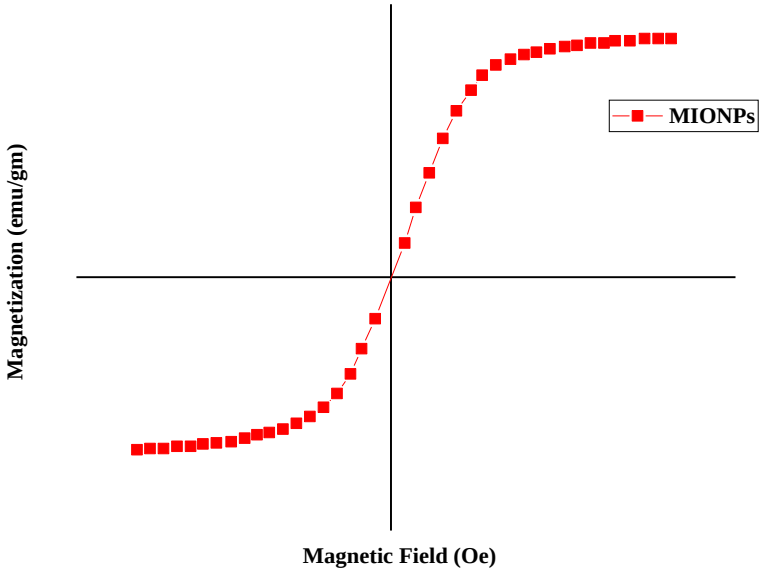

Fig. 5: Hysteresis loop of the prepared MIONPs.

3.5 Fourier Transform Infrared (FTIR) spectroscopy analysis

Fig. 6, illustrates the FTIR spectra of the synthesized MIONPs. The FTIR absorption spectra identified bands were at 3356.95, 2983.37, 1625.97, 1110.66, 1041.84, and 546.28 cm^{-1}. These bands are sought to result from vibrations, O-H stretching (3356.95 cm^{-1}), C-O bending (2983.37 cm^{-1}), and N-H stretching [24, 47]. However, the peak at 1625.97 cm^{-1} is most likely due to the bending vibrations of adsorbed water on the iron oxide surface. According to the literature, the magnetite FTIR spectrum has a strong absorption band at 570 cm^{-1} which can be attributed to the Fe-O stretching mode of the tetrahedral sites [48]. In this study, the Fe-O vibration signal of MIONPs was observed at 546.28 cm^{-1}. This shift can be attributed to the small size of the nanoparticles [25]. The weight loss seen during the thermogravimetric study provided additional evidence that the peak at 2983.37 cm^{-1} may result from C-H stretching vibrations from unreacted impurities present in the precursor salts.

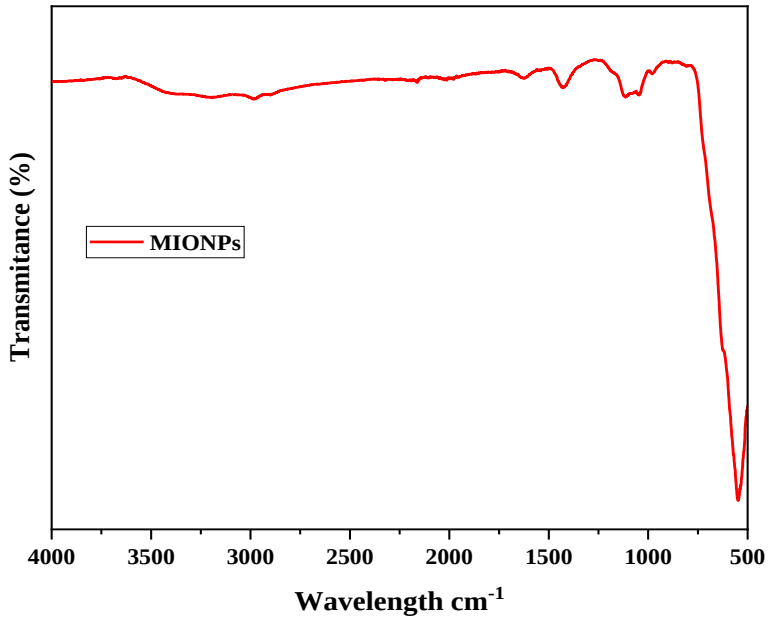

Fig. 6. FT-IR spectra for MIONPs

3.6 Thermogravimetric analysis

An important factor in determining the reaction to a mass change with temperature is the thermal property of any particular sample. Fig. 7, displays the iron oxide nanoparticle TGA curve. The curve

showed that the sample lost weight at a rate of about 1.73 wt% between 30 to 80 °C followed by 80 to 180 °C, this weight loss could be attributed to the removal of water molecules that the nanoparticles had taken from the air before the analysis [49]. After that, the sample weight remains nearly constant with a little weight loss of 2.09 wt% from a temperature range of 212 °C to 800 °C. The 2.09 wt% weight loss could also be attributed to the expulsion of trapped air within the nanoparticles crack/spaces as indicated by the SEM images in Fig.10. It may be inferred from the minimal weight loss that the synthetic MIONPs are thermally stable [50].

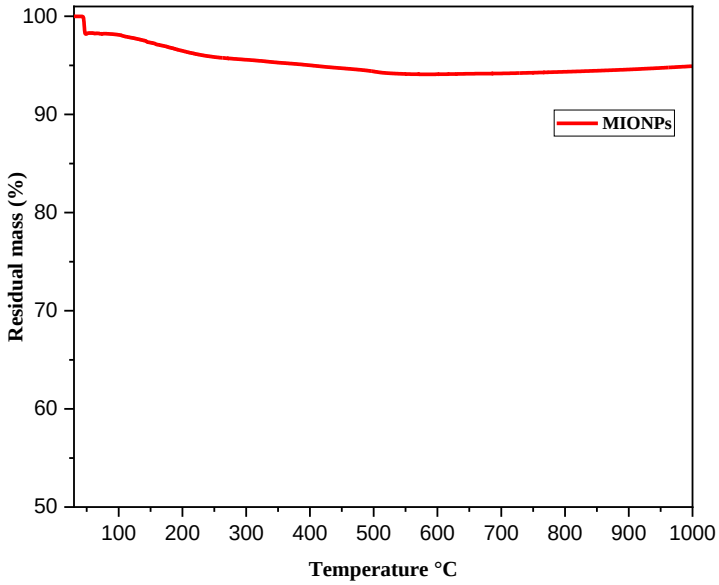

Fig. 7. Thermal properties of MIONPs

Studies reveal that the co-precipitation technique is an effective method to produce iron oxide nanoparticles such as magnetite (Fe_3O_4), hematite (α-Fe_2O_3), and maghemite (γ-Fe_2O_3) [51, 52]. The chemical reaction of Fe_3O_4 formation may be written as follows in equation 2:

$$2Fe^{3+} + Fe^{2+} + 8OH^- \rightarrow Fe_3O_4 + 4H_2O. \quad (2)$$

When the pH is between 8 and 14, it is possible to achieve complete precipitation of Fe_3O_4 with a 2:1 ratio of Fe^{3+}/Fe^{2+}. This is according to the thermodynamics of the reaction in Eq. 2. However, magnetite is not very stable and is easily oxidized. In the presence of oxygen, it changes from its black color to the brown of maghemite, even at room temperature. Under basic conditions, oxidation reactions occur on the surface of the magnetite. This means that the magnetite will be transformed into maghemite during the thermal degradation process, as long as oxygen is present on the surface of the MIONPs [53].

3.7 X-ray Diffraction (XRD) Analysis

Fig. 8, displays the X-ray diffraction patterns of the prepared MIONPs. The crystallinity and phase of the produced MIONPs were determined using the acquired XRD patterns. It is clear to discern that the X-ray diffraction patterns mainly exhibited peaks at 30.2°, 35.6°, 43.3°, 53.6°, 57.3°, and 63.0° that correspond to the magnetite reflections (220), (311), (400), (422), (511) and (440), respectively [24, 54]. These peaks indicated the existence of the crystalline spinel-structured magnetite (Fe_3O_4) phase of iron oxide, which corresponds to JCPDS number 19-629 [55]. The prepared MIONPs are suitably crystallized, as evidenced by the strong and crisp peaks. The absence of peaks from other phases demonstrates the great purity of the prepared nanoparticles. These findings are consistent with those of Rashad *et al*, 2012 [56]. As calculated using the Scherer equation, the MIONPs had a particle size of 15.21 ± 2.91 nm.

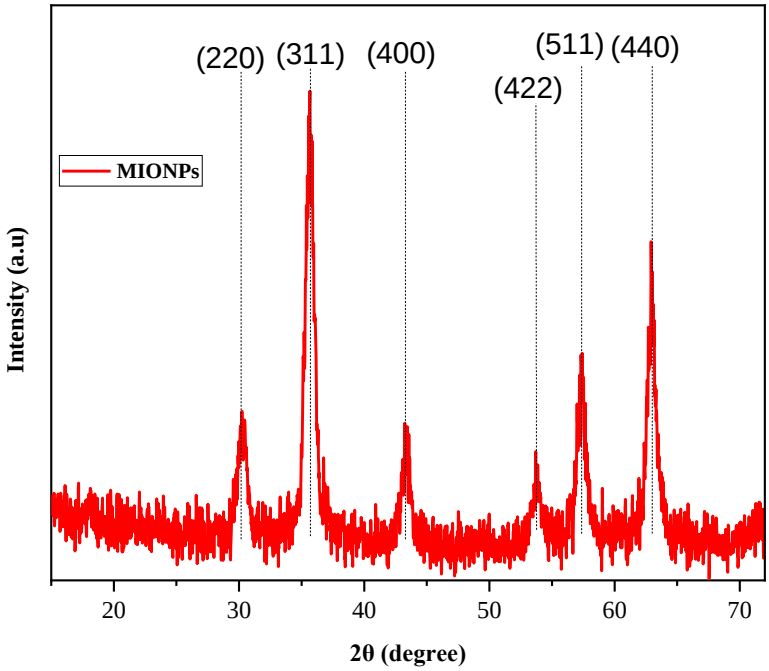

Fig. 8. XRD patterns of prepared MIONPs

3.8 Transmission Electron Microscopy

The morphological findings from the SEM data and the particle sizes from XRD were validated by transmission electron microscopy (TEM). The particle sizes, diameters, and circumferences were calculated using ImageJ (ij-153) software. Fig. 9, displays the TEM image of the prepared Fe_3O_4 nanoparticles. TEM images of Fe_3O_4 nanoparticles exhibit triangle-shaped structures, some circular and some irregular (Fig. 9a). The particles were uniformly dispersed but with agglomerations. The particles were between 6-24 nm with an average size of 16.09 ± 1.32 nm was observed (Fig. 9b). The TEM data was in agreement with the XRD data, which showed that the MIONPs had an average particle size of 15.21 ± 2.91 nm.

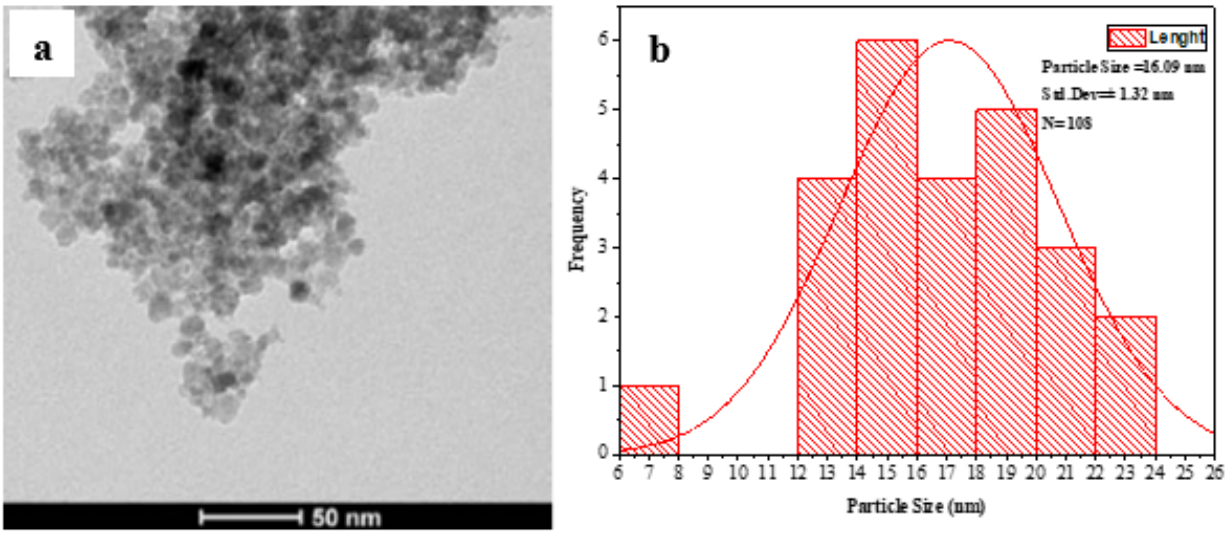

Fig. 9. TEM Micrograph and Histogram

3.9 Scanning Electron Microscopy (SEM)

Fig. 10 displays SEM images of produced nanoparticles. The nanoparticles are agglomerated together because there was no dispersion of the particles before making the SEM specimen. The agglomerations could also be linked with the use of molybdenum in aiding the precipitating process. On the other hand, the polished sample has very distinct particle boundaries. The surfaces of the

particles appear rough with tiny, invisible pores, and they appear to have non-spherical, uneven shapes and various particle sizes. Similarly, the micrographs show that the nanoparticles have sharp edges and are crystal-like, which is a clear image of magnetic nanoparticles. This is further confirmed by TEM images.

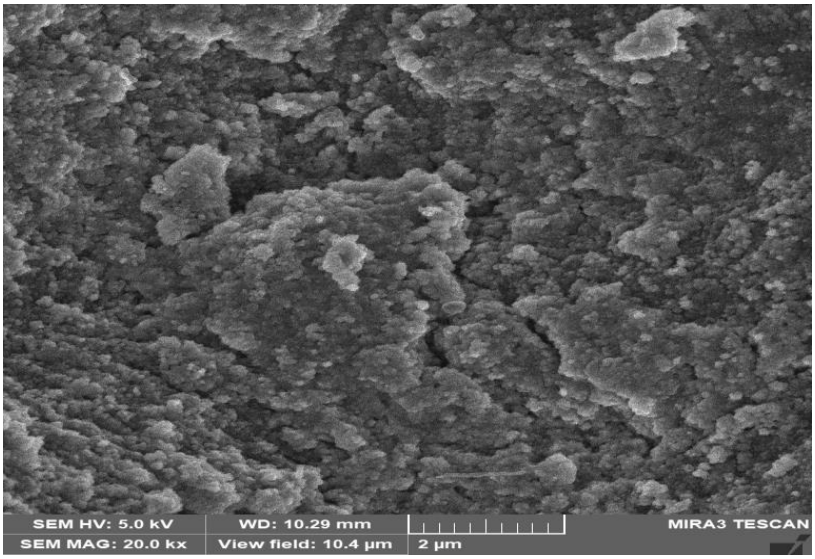

Fig.10. SEM Micrographs of MIONPs under different magnifications

3.10 Elemental Analysis

Electron Diffraction Spectroscopy (EDS) analysis was carried out to quantify the composition of various elements present in the prepared MIONPs (Fig. 11, and Table 1). The nanoparticles' chemical composition is vital in understanding their purity.

Table 1. Percentage of the elemental composition of prepared MIONPs

Element	Mass (%)	Atom (%)
C	17.81 ± 0.16	42.62 ±0.39
O	11.77 ± 0.17	21.15 ±0.31
Fe	70.41 ± 0.48	36.23 ±0.25
Total	**100.00**	**100.00**

Fig. 11, and Table 1, show the peaks that confirm the presence of Fe, O, and C with varying percentage compositions. The C is suspected to come from the EDS sample holder used during the analysis. Fe and O are the main components of MIONPs, implying that pure nanoparticles were successfully prepared. Different allotropes of iron at different binding energies (eV) were present; FeKa, FeLi, FeKb, and FeLa both comprise 70.41 ± 0.48 % of the iron salts that were used to synthesize the MIONPs. The 11.77 ± 0.17 % of oxygen resulted from the precipitating agent (NH_4OH) used during co-precipitation. This could imply that the synthesized MIONPs were pure as supported by the XRD patterns and the VSM which showed high saturation magnetization, Ms, of 74.2 emu/g. This is further supported by the strong thermal stability portrayed by the TGA curve.

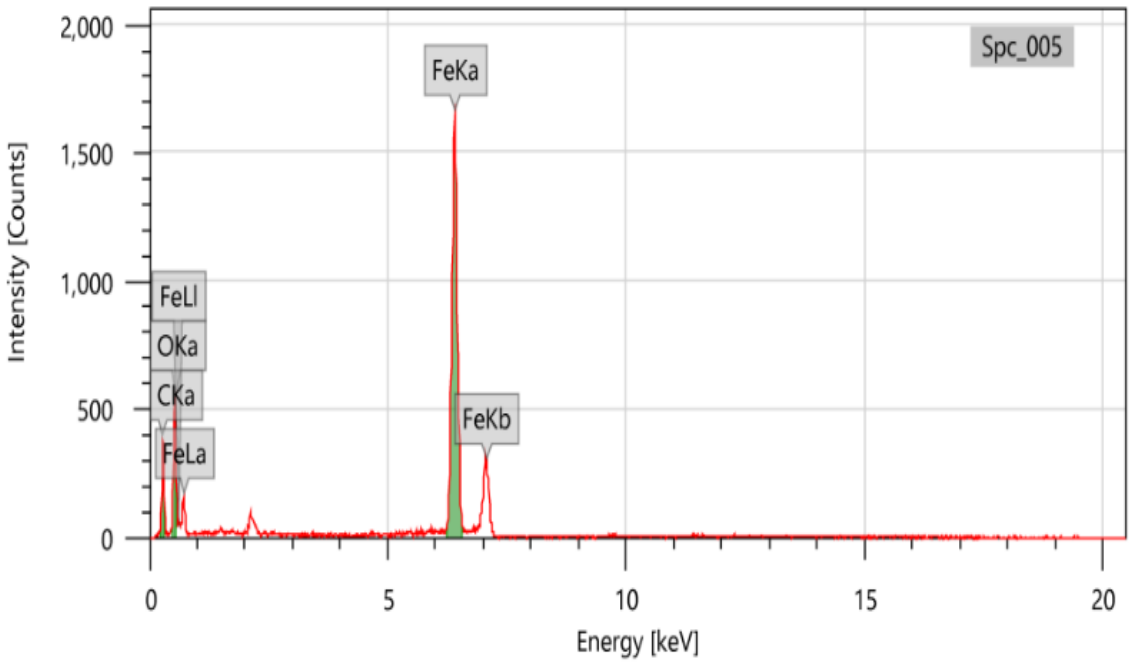

Fig.11. Elemental composition of the MIONPs

Conclusions

This study presents the synthesis and characterization of molybdenum-aided co-precipitation of stabilized magnetite iron oxide nanoparticles (MIONPs). The optical properties of the MIONPs revealed an absorptivity of 340 nm. Vibrating Sample Magnetometry (VSM) showed that the saturation magnetization of the MIONPs was 74.2 emu/g. Functional group identification indicated a high-intensity peak at 546.28 cm^{-1} ascribed to the Fe-O stretching bond. TEM scans revealed that the particles were agglomerated due to the effect of the molybdenum magnet with average particle sizes of 16.09 ±1.32 nm. This was confirmed by the XRD results that showed an average particle size of 15.21 ±2.91 nm. The synthesized iron oxide was crystalline spinel structured magnetite (Fe_3O_4) phase. EDS revealed that the major components of the produced MIONPs are Fe and O, indicating that the particles were of high purity. The results demonstrate that co-precipitation-assisted molybdenum precipitation is a viable route for the synthesis of MIONPs, and it has the potential for use in various applications.

Acknowledgments

The authors are thankful to The Vaal University of Technology for providing laboratory space, FTIR, UV-Vis, SEM-EDS, and PL analysis. The authors also acknowledge North-West University for assisting to carry out XRD, TGA, and VSM analysis. Not forgetting Dr. Lwonabo Ngodwanal for his immense assistance during the characterization.

Authors Contributions

Mr. Evans Suter contributed to the synthesis, manuscript preparation, and communication. Prof. Hilary Rutto provided the chemicals, coordinated sample characterization, and proofread the draft article. Dr. Wesley Omwoyo was engaged in the article development, PL experiments, and data analysis. Dr. Musamba Banza assisted in setting up the experiments, characterization, and proofreading the draft manuscript.

Funding

The authors have received no funding support from any institutions or organizations.

Data Availability

This article includes all of the data generated or analyzed during this research.

Compliance with Ethical Standards

Conflict of Interests

All the authors declare that they do not have any competing interests.

References

[1] P. Bradu, A. Biswas, C. Nair, S. Sreevalsakumar, M. Patil, S. Kannampuzha, & A. V. Gopalakrishnan, "Recent advances in green technology and Industrial Revolution 4.0 for a sustainable future," *Environmental Science and Pollution Research*, **2022**, 1-32. https://doi.org/10.1007/s11356-022-20024-4.

[2] D. V. Singh *et al.*, "Wonders of nanotechnology for remediation of polluted aquatic environs," *Fresh Water Pollution Dynamics and Remediation*, **2020**, 319-339. https://doi.org/10.1007/978-981-13-8277-2_17

[3] K. Yang and Y.-Q. Ma, "Computer simulation of the translocation of nanoparticles with different shapes across a lipid bilayer," *Nature Nanotechnology*, **2010**, 5(8), 579-583. https://doi.org/10.1038/nnano.2010.141.

[4] F. Trotta and A. Mele, "Nanomaterials: classification and properties," *Nanosponges Synthesis and Applications*, **2019,** 1-26. ISBN 978-3-527-34100-9

[5] V. Stone, B. Nowack, A. Baun, N. van den Brink, F. von der Kammer, M. Dusinska, R. Handy, S. Hankin, M. Hassellöv, E. Joner, and T.F. Fernandes, "Nanomaterials for environmental studies: classification, reference material issues, and strategies for physico-chemical characterisation," *Science of the total environment*, **2010**, 408(7), pp.1745-1754. https://doi.org/10.1016/j.scitotenv.2009.10.035.

[6] S. Khan, S. Mansoor, Z. Rafi, B. Kumari, A. Shoaib, M. Saeed, S. Alshehri, M.M. Ghoneim, M. Rahamathulla, U. Hani, and F. Shakeel, "A review on nanotechnology: Properties, applications, and mechanistic insights of cellular uptake mechanisms," *Journal of Molecular Liquids*, **2022**, *348*, p.118008. https://doi.org/10.1016/j.molliq.2021.118008.

[7] F. Wang, Z. Xie, H. Zhang, C. Liu, and Y. Zhang, "Highly luminescent organosilane-functionalized carbon dots," *Advanced Functional Materials*, **2011**, *21*(6), pp.1027-1031. https://doi.org/10.1002/adfm.201002279.

[8] P. Das, S. Ganguly, S. Banerjee, and N. C. Das, "Graphene based emergent nanolights: A short review on the synthesis, properties and application," *Research on Chemical Intermediates*, **2019**, *45*, pp.3823-3853. https://doi.org/10.1007/s11164-019-03823-2.

[9] S. Solgi, M. S. Seyed Dorraji, S. F. Hosseini, M. H. Rasoulifard, I. Hajimiri, and A. Amani-Ghadim, "Improvement of microwave absorption properties of polyester coatings using $NiFe_2O_4$, X-doped g-C3N4 (X= S, P, and O), and $MTiO_3$ (M= Fe, Mg, and Zn) nanofillers," *Scientific Reports*, **2021**, *11*(1), p.19339. https://doi.org/10.1038/s41598-021-98666-6.

[10] M. S. Waghmode, A. B. Gunjal, J. A. Mulla, N. N. Patil, and N. N. Nawani, "Studies on the titanium dioxide nanoparticles: Biosynthesis, applications and remediation," . *Applied Sciences*, **2019**, *1*(4), p.310. https://doi.org/10.1007/s42452-019-0337-3.

[11] S. Wahyuningsih, A. H. Ramelan, and Y. R. Kristiawan, "Transformation of Magnetite (Fe3O4) and Maghemite (γ–Fe_2O_3) to α–Fe_2O_3 from Magnetic Phase of Glagah Iron Sand," *Journal of Engineering Science,* **2019**, *15*(1), pp.11-21. https://doi.org/10.21315/jes2019.15.2.

[12] J. A. Morales-Morales, "Synthesis of hematite α-Fe_2O_3 nano powders by the controlled precipitation method," *Cienc. En Desarro,* **2017**, vol. 8, no. 1, pp. 99–107. ISSN 0121-7488

[13] P. Xu, G. Ming, D. Lian, C. Ling, S. Hu, and M. Hua, "Use of iron oxide nanomaterials in wastewater treatment: a review," A review. *Science of the Total Environment,* **2012**, 424, 1–10. https://doi.org/10.1016/j.scitotenv.2012.02.023.

[14] M. I. Anik, M. K. Hossain, I. Hossain, I. Ahmed, and R. M. Doha, "Biomedical applications of magnetic nanoparticles," in Magnetic Nanoparticle-Based Hybrid Materials, *Elsevier*, **2021**, pp. 463–497. https://doi.org/10.1016/B978-0-12-823688-8.00002-8

[15] G. M. Nair, T. Sajini, and B. Mathew, "Advanced green approaches for metal and metal oxide nanoparticles synthesis and their environmental applications," Talanta Open, **2022**, 5, p.100080. https://doi.org/10.1016/j.talo.2021.100080.

[16] W. Wu, Q. He, & C. Jiang, Magnetic iron oxide nanoparticles: synthesis and surface functionalization strategies. *Nanoscale research letters*, **2008**, 3(11), 397–415. Doi: 10.1007/s11671-008-9174-9.

[17] H. Chen and Q. Miao, "Recent advances and attempts in synthesis of conjugated nanobelts," *Journal of Physical Organic Chemistry*, **2020**, *33*(12), p.e4145. https://doi.org/10.1002/poc.4145

[18] N. Hanžić, T. Jurkin, A. Maksimović, and M. Gotić, "The synthesis of gold nanoparticles by a citrate-radiolytical method," *Radiation Physical Chemistry*, **2015**, vol. 106, pp. 77–82. https://doi.org/10.1016/j.radphyschem.2014.07.006

[19] K. S. Kim and T. H. Kim, "Nanofabrication by thermal plasma jets: From nanoparticles to low-dimensional nanomaterials," *Journal of Applied Physics,* **2019**, *125*(7), p.070901. https://doi.org/10.1063/1.5060977

[20] B. G. Pollet and M. Ashokkumar, Introduction to ultrasound, sonochemistry and sonoelectrochemistry. Springer Nature, *Springer Nature,* **2019**, pp.1-39. https://doi.org/10.1007.978-3-030-25863-7_1

[21] G. Cravotto and P. Cintas, "Power ultrasound in organic synthesis: moving cavitational chemistry from academia to innovative and large-scale applications," *Chemical Society Reviews,* **2006**, 35(2), pp.180-196. https://doi.org/10.1039/B503848K

[22] K. Hachem, M.J. Ansari, R.O. Saleh, H.H. Kzar, M.E. Al-Gazally, U.S. Altimari, S.A. Hussein, H.T. Mohammed, A.T. Hammid, and E. Kianfar, Methods of Chemical Synthesis in the Synthesis of Nanomaterial and Nanoparticles by the Chemical Deposition Method: A Review. *Bio Nanoscience,* **2022**, 12(3), pp.1032-1057. https://doi.org/10.1007/s12668-022-00996-w

[23] M. K. Yoo, I. Y. Kim, E. M. Kim, H. J. Jeong, C. M. Lee, Y. Y. Jeong, C. S. Cho, Superparamagnetic iron oxide nanoparticles coated with galactose-carrying polymer for hepatocyte targeting. *Journal of Biomedicine and Biotechnology*, **2007**, vol. 2007, https://doi.org/10.1155/2007/94740

[24] S. K. Evans, O. N. Wesley, L. Koech, S. M. Nelana, and H. L. Rutto, "Structural Features of Cellulose and Cellulose Nanocrystals via In Situ Incorporation of Magnetic Iron Oxide Nanoparticles: Modification and Characterization," *Coatings,* **2022**, vol. 13, no. 1, p. 39. https://doi.org/10.3390/coatings13010039

[25] I. Chamritski and G. Burns, “Infrared-and Raman-active phonons of magnetite, maghemite, and hematite: a computer simulation and spectroscopic study,” *Journal of Physical Chemistry B*, **2005**, vol. 109, no. 11, pp. 4965–4968. https://doi.org/10.1021/jp048748h

[26] T. Tsuzuki and P. G. McCormick, “Nanopowders synthesized by mechanochemical processing,” *Journal of Materials Science*, **2004**, vol. 39, pp. 5143–5146,. https://doi.org/10.1023/B:JMSC.0000039199.56155.f9

[27] J. Belinha, J.C. Reis Campos, E. Fonseca, M.H. Figueiral Silva, M. Arcelina Marques, M.F. Gentil Costa, and S. Oliveira, Advances and Current Trends in Biomechanics: *Proceedings of the 9th Portuguese Congress on Biomechanics*, CNB2021, 19 - 20 February 2021, Porto, Portugal (1st ed.). CRC Press. https://doi.org/10.1201/9781003217152.

[28] E. Grabias-Blicharz and W. Franus, “A critical review on mechanochemical processing of fly ash and fly ash-derived materials,” *Science of The Total Environment*, **2022**, vol. 860, p. 160529, https://doi.org/10.1016/j.scitotenv.2022.160529

[29] A. Sinha, J. Sakon, D.K. Roper, W.J. Li, A. Ghosh, H. Han, V.P. Zharov, and J.W. Kim, Nanoscale particles and multifunctional hybrid soft nanomaterials in bio/nanomedicine. In *Soft Matter and Biomaterials on the Nanoscale: The WSPC Reference on Functional Nanomaterials—Part I Volume 4: Nanomedicine: Nanoscale Materials in Nano/BioMedicine*, **2020**, pp. 1-58. https://doi.org/10.1142/9789811218026_0001

[30] H. Korbekandi, S. Iravani, and S. Abbasi, “Production of nanoparticles using organisms,” *Critical reviews in biotechnology*, **2009**, vol. 29, no. 4, pp. 279–306. https://doi.org/10.3109/07388550903062462

[31] P. A. Sundaram, R. Augustine, and M. Kannan, “Extracellular biosynthesis of iron oxide nanoparticles by Bacillus subtilis strains isolated from rhizosphere soil,” *Biotechnol. Bioprocess Engineering*, **2012**, vol. 17, pp. 835–840, 2012. https://doi.org/10.1007/s12257-011-0582-9

[32] A. Chauhan, J. Anand, V. Parkash, and N. Rai, “Biogenic synthesis: A sustainable approach for nanoparticles synthesis mediated by fungi,” *Inorganic and Nano-Metal Chemistry*, **2023**, vol. 53, no. 5, pp. 460–473. https://doi.org/10.1080/24701556.2021.2025078

[33] D. S. Mathew and R.-S. Juang, “An overview of the structure and magnetism of spinel ferrite nanoparticles and their synthesis in microemulsions,” *Chemical engineering journal*, **2007**, vol. 129, no. 1–3, pp. 51–65. https://doi.org/10.1016/j.cej.2006.11.001

[34] R. K. Kaul, P. Kumar, U. Burman, P. Joshi, A. Agrawal, R. Raliya, J.C. Tarafdar, “Magnesium and iron nanoparticles production using microorganisms and various salts,” *Material Science*, **2012**, vol. 30, pp. 254–258. https://doi.org/10.2478/s13536-012-0028-x

[35] S. Saif, A. Tahir, and Y. Chen, “Green synthesis of iron nanoparticles and their environmental applications and implications,” *Nanomaterials*, **2016,** vol. 6, no. 11, p. 209. https://doi.org/10.3390/nano6110209

[36] A. Monshi, M. R. Foroughi, and M. R. Monshi, Modified Scherrer equation to estimate more accurately nano-crystallite size using XRD. “*World Journal of Nanoscience and Engineering*, **2012**, vol.2, 154 (2012). https://doi.org/10.4236/wjnse.2012.23020

[37] R. Abu-Eittah and Z. Mobarak, “Absorption spectra of iron (III)-cannabidiolic acid solutions in organic solvents,” *Journal of Inorganic and Nuclear Chemistry*, **1972**, vol. 34, no. 7, pp. 2283–2293. https://doi.org/10.1016/0022-1902 (72)80164-7

[38] E. Posnjak and H. E. Merwin, “The system, Fe_2O_3—SO_3—H_2O,” *Journal of the American Chemical Society*, **1922,** vol. 44, no. 9, pp. 1965–1994. https://doi.org/10.1021/ja01430a016

[39] A. Ghosh, S. Dutta, I. Mukherjee, S. Biswas, S. Chatterjee, and R. Saha, "Template-free synthesis of flower-shaped zero-valent iron nanoparticle: Role of hydroxyl group in controlling morphology and nitrate reduction," *Advanced Powder Technology,* **2017**, vol. 28, no. 9, pp. 2256–2264, 2017. https://doi.org/10.1016/j.apt.2017.06.006

[40] S. Meneceur, H. Hemmami, A. Bouafia, S.E. Laouini, M.L. Tedjani, D. Berra, and M.S. Mahboub, Photocatalytic activity of iron oxide nanoparticles synthesized by different plant extracts for the degradation of diazo dyes Evans blue and Congo red. *Biomass Conversion and Biorefinery,* **2022**, pp.1-16. https://doi.org/10.1007/s13399-022-02734-4

[41] D. Shi, M. E. Sadat, A. W. Dunn, and D. B. Mast, "Photo-fluorescent and magnetic properties of iron oxide nanoparticles for biomedical applications," *Nanoscale*, **2015,** vol. 7, no. 18, pp. 8209–8232. https://doi.org/10.1039/C5NR01538C

[42] A. Gour and N. K. Jain, "Advances in green synthesis of nanoparticles", *Artificial cells, Nanomedicine, and Biotechnology,* **2019**, vol.47 (2019) pp.844–851. https://doi.org/10.1080/21691401.2019.1577878

[43] M. A. Dheyab, A. A. Aziz, M. S. Jameel, O. A. Noqta, P. M. Khaniabadi, and B. Mehrdel, "Simple rapid stabilization method through citric acid modification for magnetite nanoparticles," *Scientific Reports*, **2020**, vol. 10, no. 1, p. 10793. https://doi.org/10.1038/s41598-020-67869-8

[44] L. Maldonado-Camargo, M. Unni, and C. Rinaldi, "Magnetic characterization of iron oxide nanoparticles for biomedical applications," *Biomedical Nanotechnology Methods Protocols*, **2017,** pp. 47–71. https://doi.org/10.1007/978-1-4939-6840-4_4

[45] A. A. Dakhel, "Dielectric and optical properties of samarium oxide thin films," *Journal of alloys and compounds*, **2004,** vol. 365, no. 1–2, pp. 233–239. https://doi.org/10.1016/S0925-8388 (03)00615-7

[46] R. N. Panda, N. S. Gajbhiye, and G. Balaji, "Magnetic properties of interacting single domain Fe3O4 particles," *Journal of alloys and compounds*, **2001**, vol. 326, no. 1–2, pp. 50–53. https://doi.org/10.1016/S0925-8388 (01)01225-7

[47] B. H. Stuart, Infrared spectroscopy: fundamentals and applications. John Wiley & Sons, 2004. ISBN 0-470-85427-8

[48] M. Stoia, R. Istratie, and C. Păcurariu, "Investigation of magnetite nanoparticles stability in air by thermal analysis and FTIR spectroscopy," *Journal of Thermal Analytical Calorimetry,* **2016**, vol. 125, pp. 1185–1198. https:// doi.org//10.1007/s10973-016-5393-y

[49] R. Vijayakumar, Y. Koltypin, I. Felner, and A. Gedanken, "Sonochemical synthesis and characterization of pure nanometer-sized Fe3O4 particles," *Materials Science and Engineering A,* **2000**, vol. 286, no. 1, pp. 101–105. https://doi.org/10.1016/S0921-5093 (00)00647-X

[50] L. M. Mahlaule-Glory, S. Mapetla, A. Makofane, M. M. Mathipa, and N. C. Hintsho-Mbita, "Biosynthesis of iron oxide nanoparticles for the degradation of methylene blue dye, sulfisoxazole antibiotic and removal of bacteria from real water," *Heliyon*, **2022**, vol. 8, no. 9. https://doi.org/10.1016/j.heliyon.2022.e10536

[51] A. M. Atta, H. A. Al-Lohedan, and S. A. Al-Hussain, "Synthesis of stabilized myrrh-capped hydrocolloidal magnetite nanoparticles," *Molecules*, **2014**, vol. 19, no. 8, pp. 11263–11278. https://doi.org/10.3390/molecules190811263

[52] J.-P. Jolivet, C. Chanéac, and E. Tronc, "Iron oxide chemistry. From molecular clusters to extended solid networks," *Chemical Communications*, **2004**, no. 5, pp. 481–483. https://doi.org/10.1039/B304532N

[53] R. M. Cornell and U. Schwertmann, “The Fe Oxides: Structure, Properties,” *React. Occur. Uses VCH Weinh.* **1996**, vol. 573. https://lccn.loc.gov/96031931

[54] J. Xu, C. Ju, J. Sheng, F. Wang, Q. Zhang, G. Sun, and M. Sun, “Synthesis and characterization of magnetic nanoparticles and its application in lipase immobilization,” *Bulletin of the Korean Chemical Society*, **2013**, vol.34, no.8, pp. 2408–2412. https://doi.org/10.1016/j.jece.2022.107144

[55] I. Safitri, Y. G. Wibowo, and D. Rosarina, “Synthesis and characterization of magnetite (Fe3O4) nanoparticles from iron sand in Batanghari Beach,” in *IOP Conference Series: Materials Science and Engineering*, IOP Publishing, **2021**, p. 012020. https://doi.org/10.1088/1757-899X/1011/1/012020

[56] M. M. Rashad, H. M. El-Sayed, M. Rasly, and M. I. Nasr, “Induction heating studies of magnetite nanospheres synthesized at room temperature for magnetic hyperthermia,” *Journal of Magnetism and Magnetic Materials*, **2012**, vol. 324, no. 23, pp. 4019–4023. https://doi.org/10.1016/j.jmmm.2012.07.010